Freezing a Single Distal Motion in Dihydrofolate Reductase

Alessandro Sergi, James B. Watney, Kim F. Wong, and Sharon Hammes-Schiffer*

Department of Chemistry, 104 Chemistry Building, Pennsylvania State University, University Park, Pennsylvania 16802

Received: November 29, 2005

Constraining a single motion between distal residues separated by ∼28 Å in hybrid quantum/classical molecular dynamics simulations is found to increase the free energy barrier for hydride transfer in dihydrofolate reductase by ∼3 kcal/mol. Our analysis indicates that a single distal constraint alters equilibrium motions throughout the enzyme on a wide range of time scales. This alteration of the conformational sampling of the entire system is sufficient to significantly increase the free energy barrier and decrease the rate of hydride transfer. Despite the changes in conformational sampling introduced by the constraint, the system assumes a similar transition state conformation with a donor−acceptor distance of ∼2.72 Å to enable the hydride transfer reaction. The modified thermal sampling leads to a substantial increase in the average donor−acceptor distance for the reactant state, however, thereby decreasing the probability of sampling the transition state conformations with the shorter distances required for hydride transfer. These simulations indicate that fast thermal fluctuations of the enzyme, substrate, and cofactor lead to conformational sampling of configurations that facilitate hydride transfer. The fast thermal motions are in equilibrium as the reaction progresses along the collective reaction coordinate, and the overall average equilibrium conformational changes occur on the slower time scale measured experimentally. Recent single molecule experiments suggest that at least some of these thermally averaged equilibrium conformational changes occur on the millisecond time scale of the hydride transfer reaction. Thus, introducing a constraint that modifies the conformational sampling of an enzyme could significantly impact its catalytic activity.

I. Introduction

The role of motion in enzyme reactions has been the topic of a large number of experimental and theoretical studies.[1−3] Dihydrofolate reductase is an ideal system for studies of enzyme motion due to its relatively small size and the large amount of available experimental data.[4−8] This enzyme catalyzes the transfer of a hydride from the nicotinamide adenine dinucleotide phosphate (NADPH) cofactor to the 7,8-dihydrofolate (DHF) substrate. X-ray crystallographic structures show that the *Escherichia coli* DHFR enzyme assumes different conformations along the reaction pathway.[4] NMR relaxation experiments imply that the binding of the substrate and the cofactor induces conformational changes both in and distal to the active site.[5,9] Classical molecular dynamics simulations have been used to identify correlated and anticorrelated motions involving many of the same regions as implicated by the NMR experiments.[10] Kinetic measurements of single and multiple mutants also indicate couplings between distal regions in DHFR.[6]

Hybrid quantum/classical molecular dynamics simulations have provided evidence of a network of coupled motions extending throughout the protein and ligands.[11−13] These coupled motions represent equilibrium, thermally averaged conformational changes along the reaction coordinate. They lead to configurations that facilitate hydride transfer through short transfer distances, suitable orientation of the substrate and cofactor, and an appropriate electrostatic environment for charge transfer. Recent simulations based on alternative approaches identified similar variations in some of these geometrical properties,[14,15] and high-temperature classical molecular dynamics simulations identified nonlocal structural effects that perturb the network of coupled motions.[16] These computational studies suggest that adequate sampling of favorable equilibrium conformations plays a key role in the hydride transfer reaction catalyzed by DHFR.

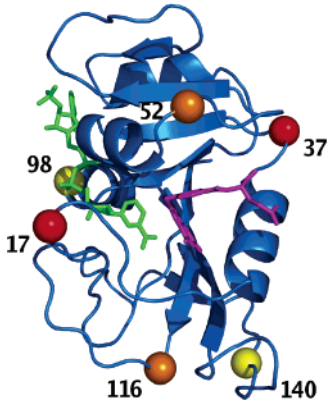

Figure 1. Secondary structure of DHFR. The NADPH cofactor is shown in green, and the DHF substrate is shown in magenta. Residues 17 and 37 are labeled with red spheres, residues 52 and 116 are labeled with orange spheres, and residues 98 and 140 are labeled with yellow spheres. In each constrained simulation, the distance between the α carbons of one of these pairs of residues was constrained.

In this paper, we apply a single distal constraint to the DHFR system and analyze the impact of this constraint on the free energy barrier and the thermally averaged reactant and transition state conformations for hydride transfer. We investigate constraints between the α carbons of three different pairs of residues separated by ∼28 Å, as illustrated in Figure 1. The choice of

* Address correspondence to this author. E-mail: shs@chem.psu.edu.

10.1021/jp056939u CCC: $33.50
Published on Web 01/13/2006

the constraint between residues Glu17 and Asp37 was motivated by recent single molecule experiments, in which these two amino acids were labeled with fluorescent probes.[17] The overall activity and hydride transfer rates were not altered by the presence of the probes. The fluorescence resonance energy transfer (FRET) was analyzed by using single molecule fluorescence microscopy under equilibrium conditions for hydride transfer. The experimental data indicate motion between residues 17 and 37 on a similar time scale as that of the hydride transfer reaction (i.e., the millisecond time scale). Our previous simulations of DHFR predicted a relatively significant change of ~0.5 Å in the thermally averaged equilibrium distance between the α carbons of residues 17 and 37 during hydride transfer.[13] This distance change is consistent with the recent single molecule experiments.[17] Note that the simulations suggest an association of this motion with hydride transfer but do not provide evidence of a causal relationship. The other two constraints investigated are between residues Arg52 and Asp116 and residues Arg98 and Phe140. Our previous simulations predicted negligible changes of less than ~0.05 Å in the thermally averaged equilibrium distances between these residues during hydride transfer.

The organization of this paper is as follows. Section II briefly summarizes the computational methodology used for the simulations and analysis. Section III presents the results, and Section IV provides a summary and conclusions.

II. Methods

The system used in our DHFR calculations contains the solvated protein, an NADPH cofactor, and a protonated DHF substrate in a truncated octahedral periodic box. The protonation of the pteridine ring was studied previously with classical free energy perturbation methods[18] and quantum mechanical methods.[19] In this paper, we focus on the hydride transfer reaction from the NADPH cofactor to the protonated DHF substrate.

The hybrid quantum/classical molecular dynamics methodology used for the present calculations is the same as the approach used previously[12,13] except for the addition of a single holonomic constraint between the α carbon atoms of the specified pair of residues. In this hybrid quantum/classical molecular dynamics approach, the electronic quantum effects are included with a two-state empirical valence bond (EVB) potential[20] based on the GROMOS force field[21] with the EVB parameters given in ref 13. The two EVB parameters corresponding to the relative energy of the two valence bond states and the coupling between these states were fit to the experimental free energies of reaction and activation.[22] In VB state 1, the hydride is bonded to its donor carbon, whereas in VB state 2, the hydride is bonded to its acceptor carbon. The nuclear quantum effects are included by representing the transferring hydrogen nucleus as a three-dimensional vibrational wave function.[23]

The free energy profile is generated as a function of a collective reaction coordinate comprised of motions from the entire solvated enzyme. This collective reaction coordinate is defined as the difference between the energies of the two VB states averaged over the lowest energy hydrogen vibrational wave function:

$$\Lambda(\mathbf{R}) = \langle \Phi_0(\mathbf{r};\mathbf{R}) | V_{11}(\mathbf{r},\mathbf{R}) - V_{22}(\mathbf{r},\mathbf{R}) | \Phi_0(\mathbf{r};\mathbf{R}) \rangle \quad (1)$$

where **r** represents the coordinate of the transferring hydrogen nucleus and **R** represents the coordinates of the remaining nuclei. $V_{11}(\mathbf{r},\mathbf{R})$ and $V_{22}(\mathbf{r},\mathbf{R})$ are the energies of VB states 1 and 2, respectively, and $\Phi_0(\mathbf{r};\mathbf{R})$ represents the ground state hydrogen vibrational wave function. This reaction coordinate has been shown to be physically meaningful for two-state charge transfer processes.[24−26] Moreover, for enzymatic reactions described within the framework of transition state theory, this reaction coordinate leads to estimates of the transmission coefficient (i.e., recrossing factor) that are close to unity.[12,27] Note that this collective reaction coordinate includes motions of the enzyme, substrate, and cofactor.

A series of mapping potentials is used to sample the relevant range of the collective reaction coordinate. These mapping potentials[20] are defined to be linear combinations of the energies of the two VB states:

$$V_{\text{map}}(\mathbf{r},\mathbf{R};\lambda) = (1 - \lambda)V_{11}(\mathbf{r},\mathbf{R}) + \lambda V_{22}(\mathbf{r},\mathbf{R}) \quad (2)$$

As the mapping parameter λ is varied from zero to unity, the reaction progresses from the reactant state to the product state. In this umbrella sampling approach, standard binning techniques are used to generate the segment of the free energy profile for each value of λ. The individual segments are connected by using thermodynamic integration to form the free energy profile corresponding to the unbiased Hamiltonian.[28] A free energy perturbation approach is used to incorporate the nuclear quantum effects into the free energy profile.[28] This procedure allows us to generate the entire adiabatic quantum free energy profile along the reaction coordinate. Note that the results presented in this paper are based on equilibrium molecular dynamics simulations, and calculations of nonequilibrium dynamical properties are not discussed here. Thus, the dynamical, time-dependent sequences of events from the motions are not provided by these simulations.

In this paper, we denote the previous hybrid quantum/classical molecular dynamics simulations[13] without an extra constraint as the "unconstrained" simulations, and we denote the present simulations in which the distance between residues *X* and *Y* is constrained as the "*X*−*Y* constrained" simulations. The extra holonomic constraint was applied with the SHAKE algorithm,[29] which was also used to apply constraints to all bonds involving hydrogen. The distance between the α carbons of the specified residues was constrained to the thermally averaged value calculated from the unconstrained simulations of the reactant.[13] The initial equilibrated structures were also obtained from these unconstrained simulations.[13]

We performed the simulations with the extra constraints for 12 different mapping potentials. For the simulations with a constraint between residues 17 and 37, we performed 500 ps of equilibration and 500 ps of data collection for each window. To test the reproducibility of the results, we repeated the entire procedure with a different initial equilibrated structure obtained from our previous unconstrained simulations. The results are similar, and the deviation of the free energy barriers from the average value is ~1 kcal/mol. The analysis of the 17−37 constrained simulations is based on the combined 1 ns of data generated from these two independent simulations. For the 52−116 and 98−140 constrained simulations, we performed 300 ps of equilibration and 200 ps of data collection for each window.

We performed a covariance analysis of the data using the procedure described in ref 13. The statistical correlation between the fluctuation of residue *j* with the fluctuation of residue *k* is given by the cross-correlation matrix[30,31]

$$S_{jk} = \frac{C_{jk}}{(C_{jj}C_{kk})^{1/2}} \quad (3)$$

where

$$C_{jk} = \langle (\mathbf{r}_j - \langle \mathbf{r}_j \rangle) \cdot (\mathbf{r}_k - \langle \mathbf{r}_k \rangle) \rangle \quad (4)$$

defines the covariance of the two fluctuations, and the brackets denote an ensemble average over configurations. The cross-correlation matrix describes pairwise atomic motions that are either in phase (i.e., moving in the same direction) or out of phase (i.e., moving in opposite directions). Relative motions that are orthogonal exhibit a cross-correlation value of zero.

We also performed a rank correlation analysis[32,33] of the data using the procedure described in ref 34. This approach identifies the correlation between a thermally averaged property along the reaction coordinate and a target model. The rank correlation approach is particularly robust and resistant to defects in the data because ranks rather than numerical values are used for the calculation of the correlations. In this paper, the thermally averaged interatomic distances along the collective reaction coordinate are correlated to a monotonically increasing linear target function from the reactant to the transition state. This approach provides a comprehensive statistical analysis of changes in thermally averaged distances along the reaction coordinate.

The covariance analysis and rank correlation analysis approaches provide information about different types of motions in the system. The degree of correlation described by the covariance analysis refers to the correlation between fluctuations of a pair of atoms about an average structure. These fluctuations are local to the average structure and typically occur on the femtosecond to picosecond time scale. In contrast, the degree of correlation in the rank correlation analysis refers to the correlation between the behavior of thermally averaged interatomic distances and a specified target model along the reaction coordinate. These motions represent changes in thermally averaged properties along the reaction coordinate and may occur on the millisecond time scale of the hydride transfer reaction.

III. Results

Our initial simulations with a single distal constraint focused on the distance between residues 17 and 37. This choice was motivated by the single molecule fluorescence experiments that identified millisecond time scale motions between these two residues. As given in Table 1, the thermally averaged distance between the α carbons of these two residues was found to change by ∼0.5 Å along the collective reaction coordinate for hydride transfer in our previous unconstrained simulations.[13] Figure 2 depicts the free energy profiles for the 17−37 constrained simulations. In general, the free energy corresponds to the probability of sampling configurations with a specified reaction coordinate. The free energy barrier arises from the lower probability of sampling transition state configurations than reactant configurations. These calculations indicate that the free energy barrier is ∼3 kcal/mol higher with the constraint than without the constraint. This increase in the free energy barrier

TABLE 1: Thermally Averaged Distances for the Reactant State, Transition State, and Product State Determined from the Unconstrained Simulations[a]

distance	reactant	transition state	product
$C_\alpha 17-C_\alpha 37$	27.79 (0.76)	28.24 (1.02)	28.16 (0.58)
$C_\alpha 52-C_\alpha 116$	28.87 (1.44)	28.74 (0.98)	28.97 (0.84)
$C_\alpha 98-C_\alpha 140$	27.92 (0.48)	27.99 (0.64)	27.97 (0.49)

[a] Distances are given in angstroms. The root-mean-square deviations are given in parentheses. $C_\alpha X-C_\alpha Y$ denotes the distance between the C_α carbons of residues *X* and *Y*.

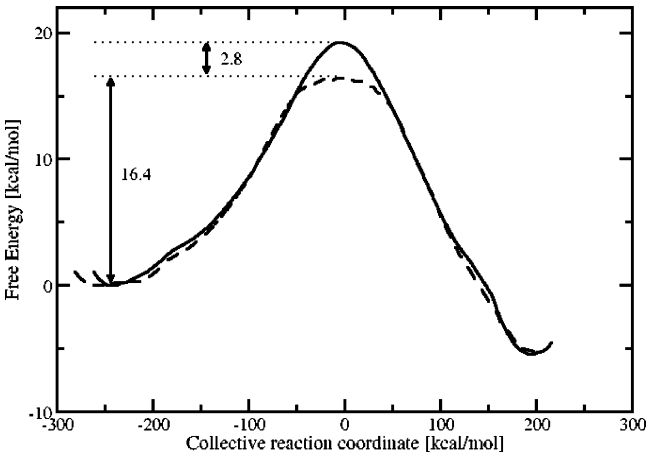

Figure 2. The free energy profiles for the hydride transfer reaction as functions of a collective reaction coordinate for the simulations in which the distance between the C_α atoms of residues 17 and 37 was constrained. The solid line indicates the classical profile, and the dashed line indicates the adiabatic quantum profile that includes the adiabatic quantum effects of the transferring hydrogen nucleus. The free energy barriers are given in kcal/mol.

implies that the single distal constraint significantly alters the conformational sampling of the entire system. Note that inclusion of nuclear quantum effects of the transferring hydrogen decreases the free energy barrier by 2.8 kcal/mol. This free energy decrease is consistent with that observed in previous simulations without the extra constraint.[12,13] Thus, the distal constraint increases the classical and adiabatic quantum free energy curves by approximately the same amount, and the effects of protein motions discussed below are not limited to quantum mechanical tunneling reactions.

We ensured that the free energy barriers for both the constrained and unconstrained simulations are reproducible. The free energy barrier obtained for the unconstrained simulations has been reproduced multiple times with different starting configurations and, in one case, starting the equilibration procedure over again from the original crystal structure. The observed changes in the free energy barrier for different starting configurations are ∼0.5 kcal/mol. Moreover, the increase in the free energy barrier with the 17−37 constraint was reproduced in two independent constrained simulations with different starting configurations. Finally, we performed an additional unconstrained simulation with the identical starting condition as used for one of the 17−37 constrained simulations, and the free energy barrier was the same as the barriers obtained in previous unconstrained simulations.

For comparison, we also calculated the free energy profiles for two pairs of residues with thermally averaged distances that do not change significantly along the collective reaction coordinate. As given by Table 1, the thermally averaged distances for the 52−116 and 98−140 pairs change by less than 0.05 Å between the reactant and the transition state. In contrast, the thermally averaged distance for the 17−37 pair changes by ∼0.5 Å. Similar to the 17−37 constrained simulations, the free energy barrier increases by ∼4 kcal/mol for the 52−116 and 98−140 constrained simulations. These results imply that the motions of residues with nearly constant thermally averaged distances also play an important role in determining the free energy barrier. Even if the thermally averaged distance between a pair of residues is constant along the collective reaction coordinate, the distance between the residues fluctuates on the femtosecond to picosecond time scale. These faster motions are washed out at equilibrium on the millisecond time scale of the

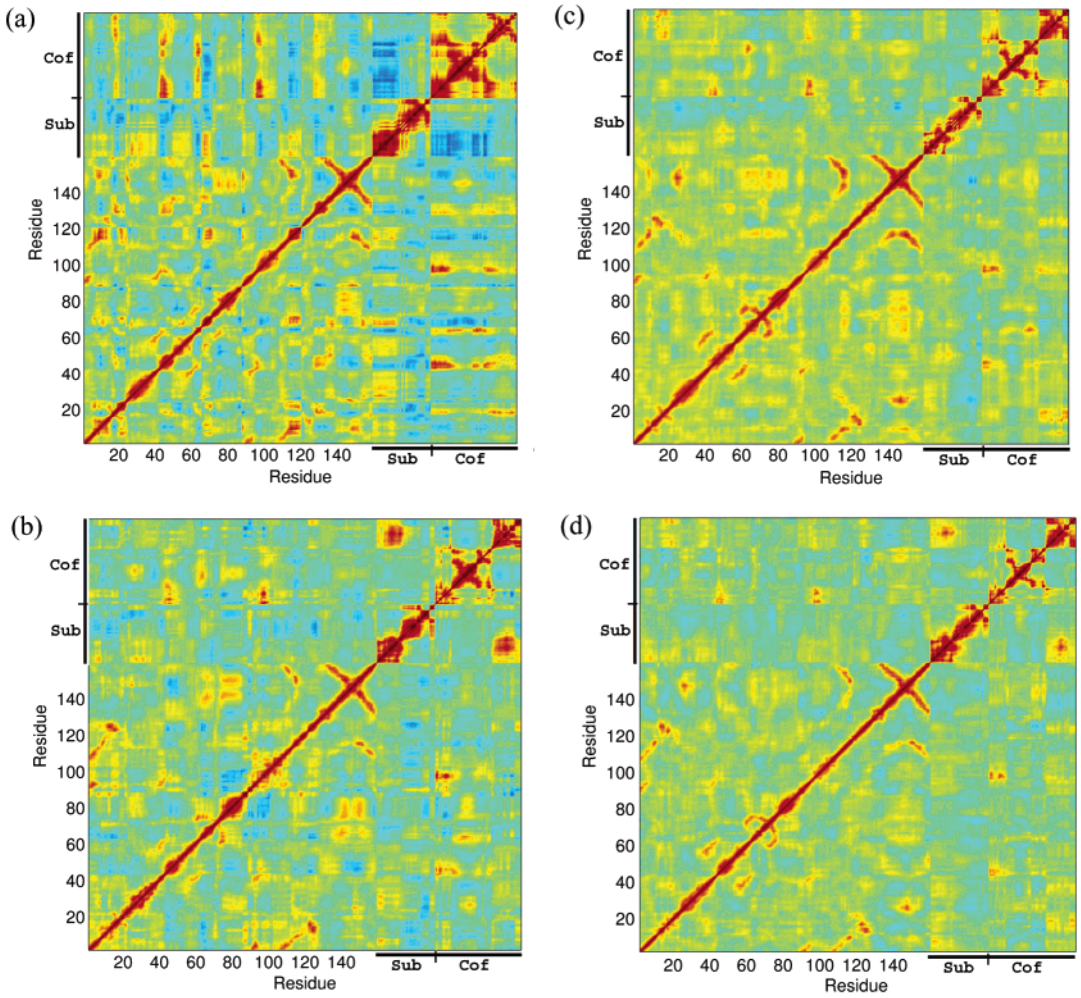

Figure 3. Covariance matrices for the C_α atoms of the DHFR enzyme and atoms of the substrate and cofactor determined for the unconstrained simulations and for the simulations in which the distance between the C_α atoms of residues 17 and 37 was constrained. Red denotes correlated regions, and blue denotes anticorrelated regions. Correlated fluctuations are illustrated for the (a) reactant state of the unconstrained simulations, (b) transition state of the unconstrained simulations, (c) reactant state of the 17−37 constrained simulations, and (d) transition state of the 17−37 constrained simulations. These matrices depict the correlation between local fluctuations of each pair of atoms about the average structure.

hydride transfer reaction, but they still impact the conformational sampling and therefore the free energy barrier.

We performed a detailed analysis of these relatively fast thermal fluctuations about the average structure. Figure 3 depicts the covariance correlation matrices for the reactant and transition state configurations obtained from the unconstrained and 17−37 constrained simulations. Although the majority of highly correlated motions (i.e., red regions) are qualitatively similar for both the unconstrained and constrained simulations, the unconstrained simulations exhibit significantly more anticorrelated motions (i.e., blue regions). Another important observation is that the highly correlated motions between the substrate and cofactor at the transition state are attenuated in the constrained simulations relative to the unconstrained simulations. These differences in the femtosecond to picosecond fluctuations about the average structure illustrate that a single distal constraint can alter the thermal fluctuations throughout the enzyme. In turn, the alteration of these fast fluctuations affects the conformational sampling leading to the slower conformational changes required for efficient hydride transfer.

We have also analyzed these thermally averaged conformational changes along the collective reaction coordinate. Figure 4 depicts the rank correlation analysis of the thermally averaged interatomic distances along the collective reaction coordinate for the unconstrained and 17−37 constrained simulations. The qualitative differences between these two correlation maps indicate that the thermally averaged equilibrium conformational changes of the enzyme occurring during hydride transfer are strongly influenced by the presence of a single distal constraint. These conformational changes along the collective reaction coordinate for hydride transfer have previously been described as forming a network of coupled motions. This network facilitates hydride transfer by bringing the donor and acceptor closer together, orienting the substrate and cofactor optimally, and providing an appropriate electrostatic environment. Single molecule fluorescence experiments have identified motions between residues 17 and 37 on the millisecond time scale.[17] These experiments suggest that at least some of the motions in this network of coupled motions occur on the millisecond time scale of the hydride transfer reaction.

Tables 2 and 3 provide selected thermally averaged geometrical parameters of the substrate and cofactor for the reactant and transition state. These geometrical parameters have been studied previously with semiempirical, ab initio, and quantum mechanical/molecular mechanical (QM/MM) methods for model systems.[19,35−39] We found that the various angles are similar for the unconstrained and constrained simulations. The most important distance determining the rate of hydride transfer is the distance between the donor and acceptor carbon atoms. Note that the root-mean-square deviation for this distance is an order

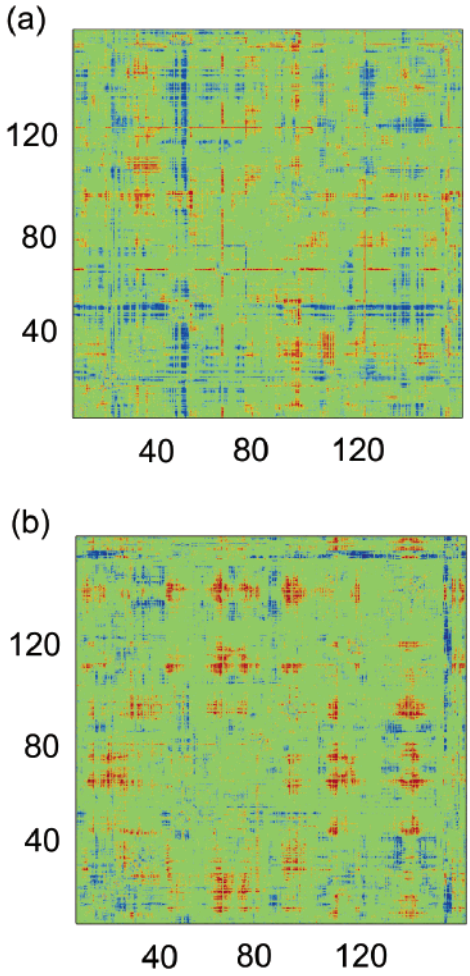

Figure 4. Rank correlation maps for the correlation of thermally averaged interatomic distances in the DHFR enzyme with a monotonically increasing linear target model along the collective reaction coordinate from the reactant to the transition state. Rank correlation maps are depicted for the (a) unconstrained simulations and (b) 17−37 constrained simulations. Red denotes correlated regions, and blue denotes anticorrelated regions. The two axes are identical and represent the amino acid sequence number of the enzyme.

of magnitude larger for the reactant state than the transition state. This observation suggests that the substrate−cofactor complex is more rigid and samples a smaller region of phase space for the transition state than for the reactant state. The thermally averaged donor−acceptor distances for the transition state span a narrow range of 2.71−2.73 Å for the unconstrained and constrained simulations. Figure 5 compares the thermally averaged transition state conformations for the unconstrained and 17−37 constrained simulations. The root-mean-square deviation for the α carbons of these two structures is only 0.71 Å. Thus, although the constraint alters the motions throughout the enzyme on a wide range of time scales, the system still must assume a similar transition state conformation to enable the hydride transfer reaction. In contrast, the thermally averaged distances between the donor and acceptor carbon atoms for the reactant state are much larger (i.e., greater than 4.0 Å). This distance is ∼1.5 Å greater for the three constrained simulations than for the unconstrained simulations. The greater average donor−acceptor distance in the reactant state decreases the probability of sampling conformations with the shorter distances required for hydride transfer and hence increases the free energy barrier for the constrained simulations.

The picture emerging from these simulations, in conjunction with previous experimental and theoretical studies, is that thermal motions of the enzyme, substrate, and cofactor lead to conformational sampling of configurations that facilitate hydride transfer. These thermal motions are Brownian in nature but occur within the confines of the enzyme structure and lead to configurations that bring the donor and acceptor closer together, orient the substrate and cofactor properly, and provide a favorable electrostatic environment. The fast femtosecond to nanosecond thermal motions are in equilibrium as the reaction progresses along the collective reaction coordinate, and the overall average equilibrium conformational changes occur on the slower time scale measured experimentally.

Figure 6 illustrates representative thermally averaged configurations from the continuous series of thermally averaged equilibrium configurations sampled along the collective reaction coordinate in the unconstrained DHFR simulations. Although the sampling was performed with mapping potentials, the thermal averages were computed by weighting each instantaneous configuration in a manner that ensured that the resulting configurations represent the thermal averages for the true potential energy surface. Note that the thermally averaged donor−acceptor distance decreases as the reaction progresses from the reactant to the transition state. The experimentally measured hydride transfer rate on the millisecond time scale corresponds to the overall rate of transformation from the equilibrium reactant configuration to the equilibrium product configuration. When the hydrogen is represented as a quantum mechanical wave function, it is delocalized between the donor and acceptor only for the relatively small number of transition state configurations.

IV. Conclusions

In this paper, we investigated the impact of freezing a single motion between distal residues in DHFR. The three pairs of residues studied (17−37, 52−116, and 98−140) are on the exterior of the enzyme and are separated by ∼28 Å. For each constrained simulation, the distance between the α carbons of the specified pair of residues was constrained to the equilibrium

TABLE 2: Thermally Averaged Distances and Angles for the Reactant State Determined from the Unconstrained Simulations and the Constrained Simulations[a]

property	unconstrained	17−37 constrained	52−116 constrained	98−140 constrained
C_D-C_A	4.01 (0.38)	5.27 (0.35)	5.53 (0.49)	5.60 (0.48)
C_D-H-C_A angle	123 (21)	113 (12)	126 (12)	124 (12)
DHF tail angle	114 (4)	114 (4)	115 (4)	115 (4)
DHF ring pucker angle	−1 (12)	−2 (11)	−5 (10)	−3 (11)
NADPH ring pucker angle	0.5 (4)	0.5 (4)	0.5 (4)	1.0 (4)

[a] Distances are given in angstroms, and angles are given in degrees. The root-mean-square deviations are given in parentheses. C_D-C_A denotes the distance between the donor and acceptor carbon atoms, and C_D-H-C_A represents the angle for these three atoms. The DHF tail angle, DHF ring pucker angle, and NADPH ring pucker angle are defined in ref 12. In the constrained simulations, the distance between the C_α atoms of the specified pair of residues was constrained.

TABLE 3: Thermally Averaged Distances and Angles for the Transition State Determined from the Unconstrained Simulations and the Constrained Simulations[a]

property	unconstrained	17−37 constrained	52−116 constrained	98−140 constrained
C_D-C_A	2.72 (0.05)	2.73 (0.04)	2.73 (0.04)	2.71 (0.04)
C_D-H-C_A angle	164 (7)	166 (6)	164 (6)	168 (6)
DHF tail angle	116 (4)	116 (4)	115 (4)	116 (4)
DHF ring pucker angle	−24 (11)	−21 (9)	−29 (7)	−2 (10)
NADPH ring pucker angle	0.3 (4)	2 (4)	0.4 (4)	−3 (4)

[a] Distances are given in angstroms, and angles are given in degrees. The root-mean-square deviations are given in parentheses. The definitions of distances and angles are the same as in Table 2. In the constrained simulations, the distance between the C_α atoms of the specified pair of residues was constrained.

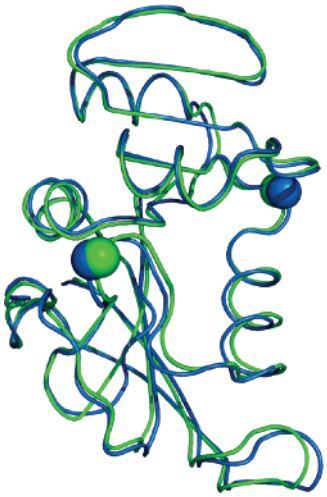

Figure 5. The thermally averaged transition state configurations for the unconstrained simulations (green) and the simulations in which the distance between the C_α atoms of residues 17 and 37 was constrained (blue). Residues 17 and 37 are labeled with spheres.

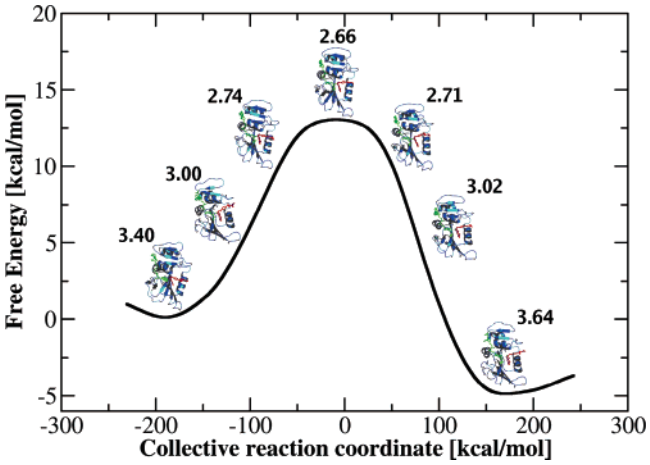

Figure 6. Free energy profile of the DHFR-catalyzed hydride transfer reaction as a function of a collective reaction coordinate that includes motions of the enzyme, substrate, and cofactor. The magnitude of the free energy barrier is determined by the relative probabilities of sampling the transition state and the reactant configurations. The thermally averaged equilibrium structures, as well as the average donor−acceptor distances in angstroms, are provided for selected values of the reaction coordinate. Note that the donor−acceptor distance decreases as the reaction evolves from the reactant to the transition state. The conformational changes along the collective reaction coordinate are attained by equilibrium thermal motions occurring within the confines of the protein fold. These conformational changes facilitate the hydride transfer reaction by bringing the donor and acceptor closer together, orienting the substrate and cofactor properly, and providing a favorable electrostatic environment.

average reactant value. In previous unconstrained simulations,[13] the thermally averaged equilibrium distance between residues 17 and 37 changed by ∼0.5 Å during hydride transfer, while the thermally averaged distances for the 52−116 and 98−140 pairs changed by less than 0.05 Å. Single molecule fluorescence experiments suggest that the changes in the thermally averaged distance between residues 17 and 37 along the collective reaction coordinate occur on the millisecond time scale of hydride transfer.

For all three pairs of residues, freezing a single distance increases the free energy barrier for hydride transfer by 3−4 kcal/mol. Even if the thermally averaged distance between a pair of residues is constant during the reaction, the distance between the residues fluctuates thermally on the femotosecond to picosecond time scale. These fast fluctuations are averaged out at equilibrium on the millisecond time scale of the hydride transfer reaction. Altering these fast fluctuations affects the thermal sampling, however, which in turn impacts the slower equilibrium conformational changes required to facilitate hydride transfer. Our analyses indicate that a constraint between distal residues impacts equilibrium motions throughout the enzyme on a wide range of time scales spanning femtoseconds to milliseconds. This alteration of the conformational sampling of the entire system is sufficient to significantly increase the free energy barrier and decrease the rate of hydride transfer.

We also studied the impact of a distal constraint on the thermally averaged reactant and transition state structures. Our analysis focused mainly on the distance between the donor and acceptor carbon atoms. The average donor−acceptor distance for the transition state was ∼2.72 Å for the unconstrained simulations and was not altered significantly in the presence of a single distal constraint. Despite the changes in conformational sampling introduced by the constraint, the system must still assume a similar transition state conformation to enable the hydride transfer reaction. In contrast, the average donor−acceptor distance for the reactant state was ∼4.0 Å for the unconstrained systems and ∼5.5 Å for the constrained simulations. The alteration of the thermal sampling introduced by the constraint significantly increases the average donor−acceptor distance for the reactant state, thereby decreasing the probability of sampling conformations with the shorter distances required for hydride transfer. As a result, the free energy barrier is substantially higher in the presence of a single distal constraint.

The general picture emerging from these simulations is that thermal fluctuations of the enzyme, substrate, and cofactor lead to conformational sampling of configurations that facilitate hydride transfer. These thermal motions are Brownian in nature but have restraints imposed by the enzyme structure. They lead to configurations that bring the substrate and cofactor closer together, orient them properly, and provide a favorable electrostatic environment for hydride transfer. The fast femtosecond to nanosecond thermal motions are in equilibrium as the reaction progresses along the collective reaction coordinate, and the

overall average equilibrium conformational changes occur on the slower time scale measured experimentally. The recent single molecule experiments[17] confirm that at least some of these thermally averaged equilibrium conformational changes occur on the millisecond time scale of the hydride transfer reaction. Within this framework, introducing a constraint that modifies the conformational sampling of the enzyme could significantly impact its catalytic activity.

Acknowledgment. We gratefully acknowledge Steve Benkovic and Gordon Hammes for helpful discussions and for sharing their single molecule data prior to publication. This work was supported by National Institutes of Health Grant GM56207.

References and Notes

(1) Tousignant, A.; Pelletier, J. N. *Chem. Biol.* **2004**, *11*, 1037.
(2) Benkovic, S. J.; Hammes-Schiffer, S. *Science* **2003**, *301*, 1196.
(3) Klinman, J. P. *Pure Appl. Chem.* **2003**, *75*, 601.
(4) Sawaya, M. R.; Kraut, J. *Biochemistry* **1997**, *36*, 586.
(5) Osborne, M. J.; Schnell, J.; Benkovic, S. J.; Dyson, H. J.; Wright, P. E. *Biochemistry* **2001**, *40*, 9846.
(6) Rajagopalan, P. T. R.; Lutz, S.; Benkovic, S. J. *Biochemistry* **2002**, *41*, 12618.
(7) Sikorski, R. S.; Wang, L.; Markham, K. A.; Rajagopalan, P. T. R.; Benkovic, S. J.; Kohen, A. *J. Am. Chem. Soc.* **2004**, *126*, 4778.
(8) Maglia, G.; Allemann, R. K. *J. Am. Chem. Soc.* **2003**, *125*, 13372.
(9) Schnell, J. R.; Dyson, H. J.; Wright, P. E. *Biochemistry* **2004**, *43*, 374.
(10) Radkiewicz, J. L.; Brooks, C. L. *J. Am. Chem. Soc.* **2000**, *122*, 225.
(11) Agarwal, P. K.; Billeter, S. R.; Rajagopalan, P. T. R.; Benkovic, S. J.; Hammes-Schiffer, S. *Proc. Natl. Acad. Sci. U.S.A.* **2002**, *99*, 2794.
(12) Agarwal, P. K.; Billeter, S. R.; Hammes-Schiffer, S. *J. Phys. Chem. B* **2002**, *106*, 3283.
(13) Wong, K. F.; Watney, J. B.; Hammes-Schiffer, S. *J. Phys. Chem. B* **2004**, *108*, 12231.
(14) Garcia-Viloca, M.; Truhlar, D. G.; Gao, J. *Biochemistry* **2003**, *42*, 13558.
(15) Thorpe, I. F.; Brooks, C. L., III *J. Phys. Chem. B* **2003**, *107*, 14042.
(16) Swanwick, R. S.; Shrimpton, P. J.; Allemann, R. K. *Biochemistry* **2004**, *43*, 4119.
(17) Antikainen, N. M.; Smiley, R. D.; Benkovic, S. J.; Hammes, G. G. *Biochemistry* **2005**, *44*, 16835.
(18) Singh, U. C. *Proc. Natl. Acad. Sci. U.S.A.* **1988**, *85*, 4280.
(19) Cummins, P. L.; Gready, J. E. *J. Am. Chem. Soc.* **2001**, *123*, 3418.
(20) Warshel, A. *Computer Modeling of Chemical Reactions in Enzymes and Solutions*; John Wiley & Sons: New York, 1991.
(21) van Gunsteren, W. F.; Billeter, S. R.; Eising, A. A.; Hunenberger, P. H.; Kruger, P.; Mark, A. E.; Scott, W. R. P.; Tironi, I. G. *Biomolecular simulation*: *The GROMOS96 manual and user guide*; VdF Hochschulverlag, ETH Zurich: Zurich, Switzerland, 1996.
(22) Fierke, C. A.; Johnson, K. A.; Benkovic, S. J. *Biochemistry* **1987**, *26*, 4085.
(23) Webb, S. P.; Hammes-Schiffer, S. *J. Chem. Phys.* **2000**, *113*, 5214.
(24) Marcus, R. A. *Annu. Rev. Phys. Chem.* **1964**, *15*, 155.
(25) Zusman, L. D. *Chem. Phys.* **1980**, *49*, 295.
(26) Warshel, A. *J. Phys. Chem.* **1982**, *86*, 2218.
(27) Billeter, S. R.; Webb, S. P.; Agarwal, P. K.; Iordanov, T.; Hammes-Schiffer, S. *J. Am. Chem. Soc.* **2001**, *123*, 11262.
(28) Billeter, S. R.; Webb, S. P.; Iordanov, T.; Agarwal, P. K.; Hammes-Schiffer, S. *J. Chem. Phys.* **2001**, *114*, 6925.
(29) Ryckaert, J. P.; Ciccotti, G.; Berendsen, H. J. C. *J. Comput. Phys.* **1977**, *23*, 327.
(30) Ichiye, T.; Karplus, M. *Proteins*: *Struct., Funct., Genet.* **1991**, *11*, 205.
(31) Kitao, A.; Go, N. *Curr. Opin. Chem. Biol.* **1999**, *9*, 164.
(32) Press: W. H.; Teukolsky, S. A.; Vetterling, W. T.; Flannery, B. P. *Numerical Recipes in Fortran 77*: *The Art of Scientific Computing*, 2nd ed.; Cambridge University Press: New York, 1992.
(33) Lehmann, E. L. *Nonparametrics*: *Statistical Methods Based on Ranks*; Holden-Day: San Francisco, CA, 1975.
(34) Wong, K. F.; Selzer, T.; Benkovic, S. J.; Hammes-Schiffer, S. *Proc. Natl. Acad. Sci. U.S.A.* **2005**, *102*, 6807.
(35) Cummins, P. L.; Gready, J. E. *J. Comput. Chem.* **1990**, *11*, 791.
(36) Cummins, P. L.; Gready, J. E. *J. Comput. Chem.* **1998**, *19*, 977.
(37) Castillo, R.; Andres, J.; Moliner, V. *J. Am. Chem. Soc.* **1999**, *121*, 12140.
(38) Andres, J.; Moliner, V.; Safont, V. S.; Domingo, L. R.; Picher, M. T.; Krechl, J. *J. Bioorg. Chem.* **1996**, *24*, 10.
(39) Andres, J.; Safont, V. S.; Martins, J. B.; Beltran, A.; Moliner, V. *J. Mol. Struct.*: *THEOCHEM* **1995**, *330*, 411.